FINAL REPORT

DUAL CHANNEL REMOTE INFRARED THERMOGRAPHER

CONTRACT NO: F33615-00-M-6035

MARCH, 2001

Submitted to:

Air Force Research Laboratory / HEDR
8308 Hawks Road, Bldg, 1184
Brooks AFB, 78235-5368

Submitted by:

OPTRA, Inc.
461 Boston Street
Topsfield, MA 01983

Principal Investigator

Julia Rentz

20010320 107

OPTRA

REPORT DOCUMENTATION PAGE		Form Approved OMB No. 0704-0188

Public reporting burden for this collection of information is estimated to average 1 hour per response, including the time for reviewing instructions, searching existing data sources, gathering and maintaining the data needed, and completing and reviewing the collection of information. Send comments regarding this burden estimate or any other aspect of this collection of information , including suggestions for reducing this burden to Washington Headquarters Services, Directorate for Information Operations and Reports, 1215 Jefferson Davis Highway, Suite 1204, Arlington, VA 22202-4302, and to the Office of Management and Budget, Paperwork Reduction Project, Washington, DC 20503

1. AGENCY USE ONLY (Leave blank)	2. REPORT DATE 10-Feb-01	3. REPORT TYPE AND DATES COVERED Final - 5/18/00 - 2/18/01

4. TITLE AND SUBTITLE Dual Channel Remote Infrared Thermographer	5. FUNDING NUMBERS Contract F33615-00-M-6035
6. AUTHOR(S) Julia H. Rentz	
7. PERFORMING ORGANIZATION NAME(S) AND ADDRESS(S) OPTRA, Inc. 461 Boston Street Topsfield, MA 01983	8. PERFORMING ORGANIZATION REPORT UNMBER 202
9. SPONSORING/MONITORING AGENCY NAME(S) AND ADDRESSES(S) Department of the Air Force 2310 Eight Street, Bldg 167 Wright-Patterson AFB, OH 45433-7801	10. SPONSORING/MONITORING AGENCY REPORT NUMBER
11. SUPPLEMENTAL NOTES	
12a. DISTRIBUTION / AVAILABILITY STATEMENT Approved for public release; SBIR report, distribution unlimited	12b. DISTRIBUTION CODE

13. ABSTRACT *(Maximum 200 words)*

Report developed under SBIR contract for Topic AF00-095
This report summarizes Phase I proof of feasibility work on our dual channel remote thermographer for the measurement of human skin temperature. We have successfully demonstrated a color temperature measurement using two infrafed interference filters with neighboring spectral passbands alternating in front of an uncooled amorphous silicon microbolometer detector. The normalized difference between the two channels provides an emissivity-independent measurement of the spectral shift in the Planck profile associated with the temperature of the target. This concept was demonstrated with a breadboard system comprised of off-the-shelf filters and a 10" f/4.5 Newtonian telescope at a standoff of 30m. The performance evaluation measured the system response to a controlled blackbody, NEDT,accuracy, field of view, and human skin temperature. The Phase I effort also produced a calibration routine to correct for water vapor in the measurement path as well as changes in background radiation. We also formulated a system cost model. Phase I continuity activities included a review of the Phase I findings as well as the beginning of the Phase II Preliminary Design.

14. SUBJECT TERMS Thermographer Thermometer Infrared	 Radiometer Microbolometer SBIR Report	15. NUMBER OF PAGES 34 16. PRICE CODE
17. SECURITY CLASSIFICATION OF REPORT	Unclassified	20. LIMITATION OF ABSTRACT UL

Standard Form 298

TABLE OF CONTENTS

LIST OF FIGURES

LIST OF TABLES

1.0 INTRODUCTION

1.1 Purpose of This Research

The U.S. Air Force has presented us with the opportunity to develop an accurate remote infrared thermographer for measuring human skin temperature at large standoffs. This system must be capable of resolving a small spatial area at a standoff of 1 km, which means a very small field of view. At the same time, this system must offer sufficient accuracy ($\pm$ 1°C), which is ultimately limited by the noise equivalent temperature (NEΔT) of the thermographer. This system must also be insensitive to changes in background radiation as well as the effects of water vapor in the path of the measurement. The current state of this technology measures the temperature-dependent spectrally-integrated radiance of a target using infrared optics and infrared detectors. As discussed in the following sub-section, the technology presently available falls short of meeting the functional requirements of this application because of its limited accuracy, sensitivity to target emissivity, and large spot size at the requisite standoff. Moreover, most of these systems also do not address the effects of water vapor in the measurement path.

We proposed and experimentally demonstrated the feasibility of a color temperature measurement to address this application. Our system consists of two infrared channels defined by two interference filters with neighboring passbands alternating in front of an uncooled amorphous silicon (a-Si) microbolometer. The difference in measured radiance between the two channels is proportional to the temperature-dependent peak wavelength of the spectrum emitted from the target. Normalizing the difference signal by the sum of the two channels makes the measurement independent of target emissivity. We demonstrated this concept during the Phase I using off-the-shelf IR filters and an f/4.5 10-inch Newtonian telescope with a standoff of about 30 meters.

1.2 Background

Current IR thermometer technology is based on the concept that IR radiation is proportional to the temperature of the body from which it is emitted according to Planck's blackbody description. These systems employ IR collection optics and one of a number of different IR detectors such as germanium, silicon, lead selenide, mercury cadmium telluride, and indium gallium arsenide which are photoelectric devices or bolometers, pyroelectric detectors, and thermopiles which are thermal devices. These systems are available over most temperature ranges but require knowledge of the emissivity of the target. These systems are also limited in accuracy, resolution, and spot size at large standoff distances. Table 1 lists some commercially available IR thermometers.[1,2,3,4,5,6]

[1] www.alfaelectronics.com/TM908.HTML
[2] www.batech-jp.com/bt-e.html
[3] www.geneq.com/catalog/en/it.htm
[4] mitchellinstrument.com/HotspotInfraredThermomet.html
[5] www.omega.ca/ce/products/os520.html
[6] www.sj-electronics.co.uk/DATA%20SHEETS/fluke_65.htm

Table 1: Matrix of Comparable Technologies

Manufacturer	Model	Temperature Range (°c)	Resolution (°c)	Accuracy (°c)	Spot Size At 100m (m)	Emissivity	Response Time (s)	Size (in)
Alfa Elect.	TM-908	-10 to 300	.1 or 1	±2	14.3	.1 to .95	1	7.1×2.8×1.3
Batech	BT1000	-20 to 300	.1 to 1	±3.2	0.5	.3 to .95	.25	3.2×5.6×1.2
Geneq	Quick Temp	-18 to 315	1	±2	33.0	.95	1	7.3×1.7×.75
Michell Inst.	Hot Spot	-50 to 1000	1	±8.4	2.5	-	.75	Hand-held
Omega	OS520	-18 to 540	1	±5.6	5.0	.1 to 1.0	.25	Hand-held
S.J. Elect Ltd	Fluke 65	-40 to 500	.1 to 1	±2 to ±5	12.5	.95	-	Hand-held

1.3 Key Innovations

OPTRA has developed a new approach to infrared thermography. We have demonstrated a spectral temperature measurement using two infrared channels with adjacent spectral passbands which measure the temperature-dependent peak wavelength of the spectrum emitted from a target. The normalized difference between the measured radiance of the two channels is proportional to temperature and independent of target emissivity. Our system utilizes an uncooled amorphous silicon microbolometer detector which offers higher detectivity than pyroelectric or other bolometric uncooled detectors. We have demonstrated a breadboard scale Phase I system using a 10-inch f/4.5 Newtonian telescope and a corresponding 0.1° field of view of our instrument, allowing for the accurate measurement of skin temperature of a 5-cm target area at a 30 m standoff.

1.4 Technical Objectives

The Technical Objectives accomplished during the Phase I work effort are listed below with a few short statements describing how each was met.

1. Procure Two Infrared Filters with Neighboring Passbands
We selected and procured the two filters from Optical Coatings Laboratories, Inc. (OCLI) after having evaluated their passbands in our system performance model. The respective passbands are 8-11.2 μm and 9.5-12.6 μm.

2. Design and Breadboard Thermographer
We designed the opto-mechanical and electrical systems of our Phase I system incorporating the selected filters, the microbolometer, the telescope, and the lock-in amplifier. All sub-system designs are described and pictured In the body of this report.

3. *Formulate Calibration Routine*

A calibration routine was formulated based on the selected system components. This routine will correct for an offset due to the presence of water vapor in the measurement path as well as changes in the sensor's internal temperature.

4. *Test Thermographer for NEΔT, Accuracy, and FOV*

The thermographer was tested for NEΔT, accuracy, and field of view, and the results were compared to those predicted by the model. Results are given in the body of this report.

5. *Test Thermographer on Human Subject*

The temperature of a human subject was measured at a 30 m standoff with the Phase I breadboard. The results are given in the body of this report.

6. *Formulate System Cost Model*

A system cost model was developed for the final prototype described in the Phase II proposal. This cost model is given later in the body of this report.

The Technical Objectives designated for the Phase I Continuity activities are as follows.

1. *Review Phase I Findings*

The test results were carefully reviewed, and necessary recommendations were made with regard to the Phase II system.

2. *Review Optical / Mechanical / Electrical Systems*

The following issues borne from the Phase I research were addressed on a conceptual level under this objective: atmospheric attenuation, calibration, temperature logging, and aiming. Each issue is described and addressed in the body of this report.

3. *Begin Preliminary Design*

The start of a preliminary design is marked by a Conceptual Design, which we made some progress towards at the end of the Phase I Continuity period. Conceptual Designs for each of the relevant subsystems are presented in the body of this report.

2.0 SUMMARY OF PHASE I WORK

2.1 Introduction

The purpose of the Phase I was to conduct a feasibility study on the proposed color temperature measurement. We proposed to accomplish this task through the design and build of a breadboard system which would be tested for NEΔT, accuracy, and field of view.

Figure 1 depicts the Phase I system concept. Infrared light from a target is collected by the Newtonian telescope and is focused through the alternating infrared filters and onto the microbolometer detector. The beam is amplitude modulated by an optical chopper (necessary for the AC-coupled microbolometer and synchronous detection scheme). The microbolometer output signals (corresponding to each filter transmission) are sent into the lock-in amplifier for synchronous detection along with the chopper frequency reference. The two signals are subtracted at each temperature and divided by the difference, yielding an emissivity-insensitive temperature measurement.

Figure 1: Phase I System Concept

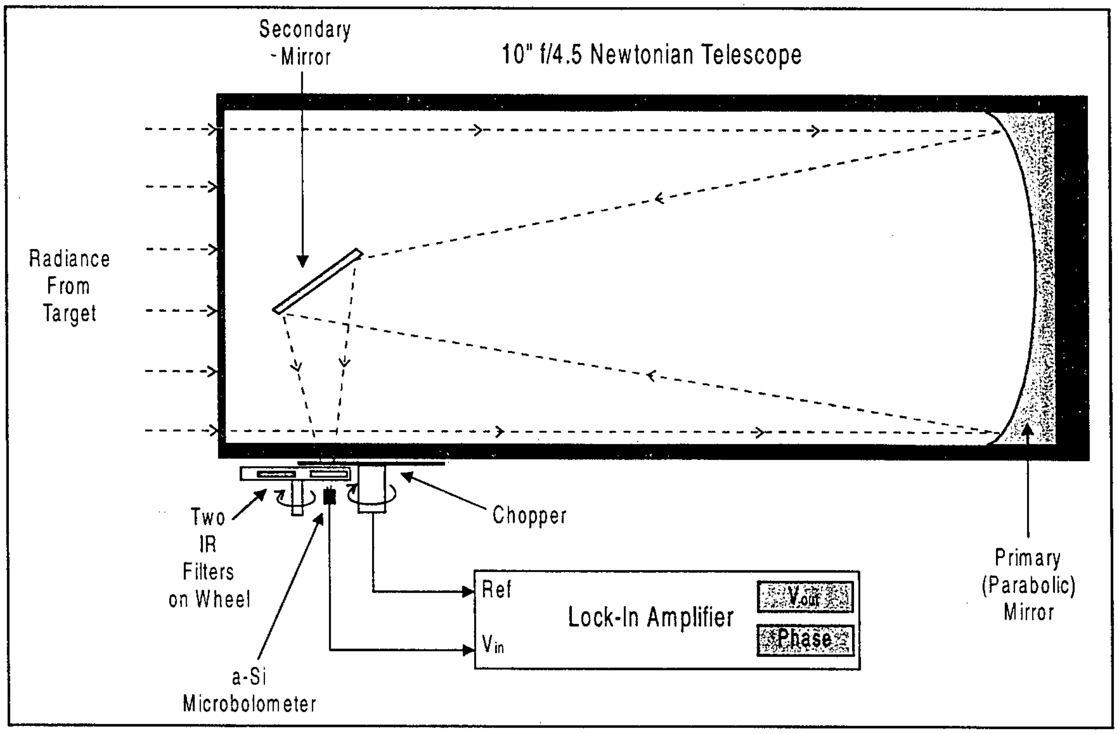

The following presents a thorough representation of the work performed under this Phase I contract. An overview of the proposed technology is presented. The systems analysis done for this project is presented. Optical, mechanical, and electrical system designs are presented and depicted. System tests are described, and results are given.

2.2 Phase I Systems Analysis

The system analysis conducted at the beginning of the Phase I produced a prediction of system performance and the basis for calibration. The following summarizes this analysis performed in MathCAD.

2.2.1 The Filters

The filter selection process made careful consideration of the water vapor absorption profile in the 8 to 12 µm spectral region. The goal was to balance out of the effects of water vapor absorption in each channel. The selected filters' characteristics are given in table 2; the filter data provided by the vendor is shown in figure 2. Both filters were purchased from OCLI.

Table 2: IR Filter Characteristics

FILTER NO.	λ_{center}	λ_{lower}	λ_{upper}	$\delta\lambda$	T
1	9.592 µm	8.01 µm	11.17 µm	3.16 µm	89%
2	11.02 µm	9.51 µm	12.60 µm	3.09 µm	80%

Figure 2a and 2b: IR Filters 1 and 2 Data

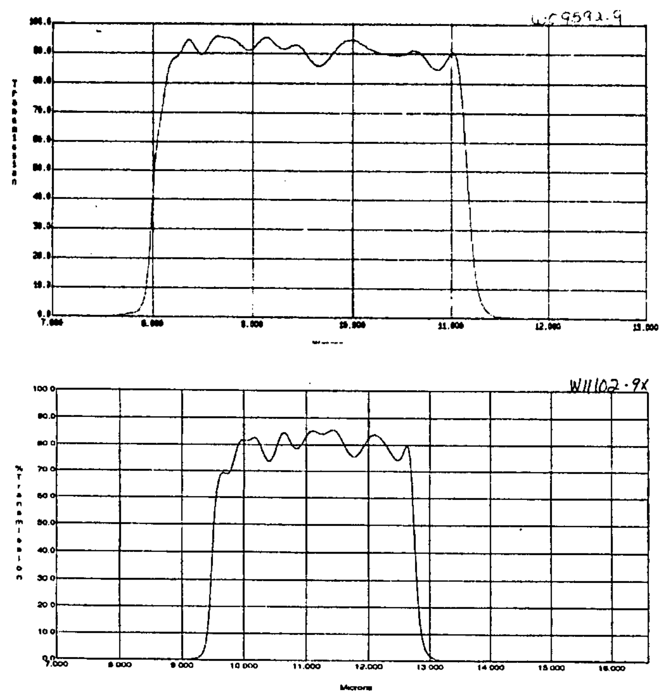

The filter profiles are superimposed against the water vapor bands in figure 3 to depict the balanced passbands. The water vapor concentration pathlength shown in the figure is 0.1 atm·m or 1% water vapor over a 10 m pathlength; the profiles were generated using the Hitran spectral database.[7] In general, this is a low-attenuation region in comparison to the mid-IR.

Figure 3: IR Filter and Water Vapor Profiles

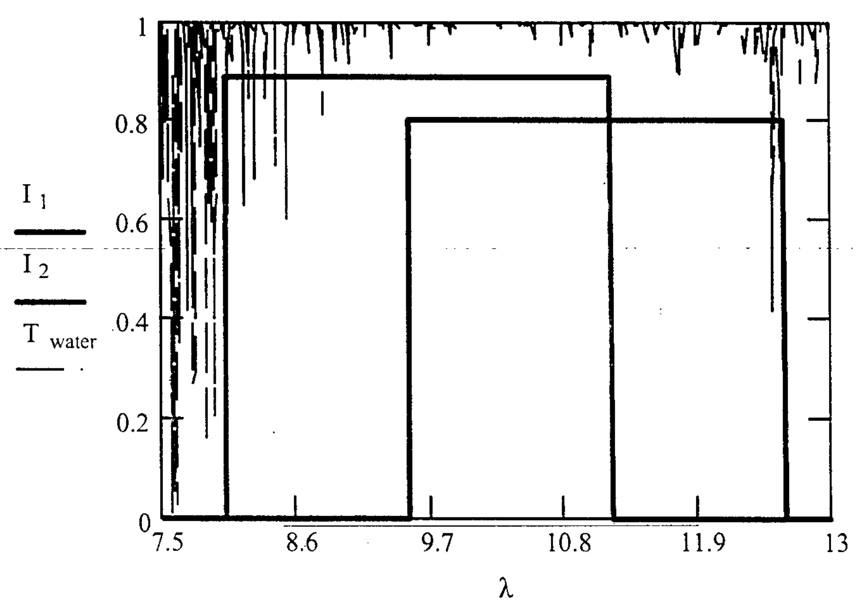

[7] Ontar Corporation, 9 Village Way, North Andover, MA 01845-2000.

2.2.2 The Signals

The transmitted radiance through each filter is given by

$$S_1(T) = \int_\lambda I_1(\lambda) \cdot \varepsilon \cdot N(\lambda, T) d\lambda \qquad (1a) \qquad\qquad S_2(T) = \int_\lambda I_2(\lambda) \cdot \varepsilon \cdot N(\lambda, T) d\lambda \qquad (1b)$$

where $\varepsilon \cdot N$ is the emissivity multiplied by the spectral radiance of the target, which is given by

$$N(\lambda, T) = \frac{c_1}{\lambda^5} \cdot \left(e^{\frac{c_2}{\lambda T}} - 1 \right)^{-1} \qquad (2)$$

$c_1 = 2 \cdot h \cdot c$ where h is Planck's constant (6.626×10^{-34} J·s) and c is the speed of light (3×10^{10} cm/s). $c_2 = h \cdot c/k$ where k is Boltzman's constant (1.381×10^{-23} J/K). In the *absence of water vapor*, the normalized thermographer output signal is proportional to

$$S_{output}(T) = \frac{S_1(T) - S_2(T)}{S_1(T) + S_2(T)} \qquad (3)$$

Figure 4 shows the predicted response of the Phase I system over the 15 to 45°C (288 – 318 K) temperature range.

Figure 4: Phase I System Predicted Response

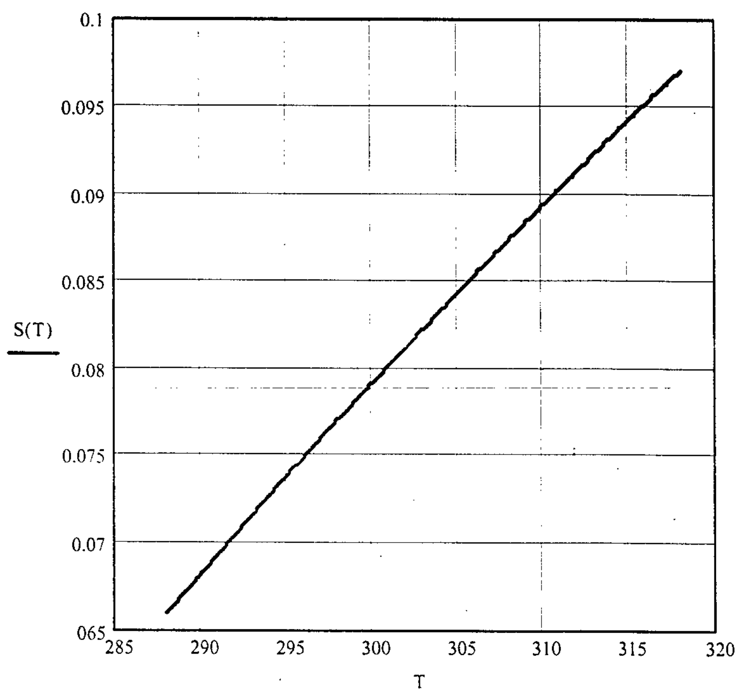

The thermographer output will be somewhat affected by water vapor attenuation, however. In this case, equations 1a and 1b become

$$S_1(T) = \int_\lambda I_1(\lambda) \cdot \varepsilon \cdot N(\lambda, T) \cdot \tau_{wv}(\lambda) d\lambda \qquad (4a) \qquad\qquad S_2(T) = \int_\lambda I_2(\lambda) \cdot \varepsilon \cdot N(\lambda, T) \cdot \tau_{wv}(\lambda) d\lambda \qquad (4b)$$

where $\tau(\lambda)$ is the water vapor profile given by

$$\tau_{wv}(\lambda) = e^{-\sigma(\lambda)CL} \qquad (5)$$

$\sigma(\lambda)$ is the wavelength-dependent absorption cross section which may be acquired through any one of a number of spectral data bases (such as Hitran).

The final effect to the system performance is a slight shift in the response as shown in figure 5. As will be explained in the *Phase I Review*, we intend to address this issue by means of a relative humidity measurement and a correction lookup table.

Figure 5: Water Vapor Look-up

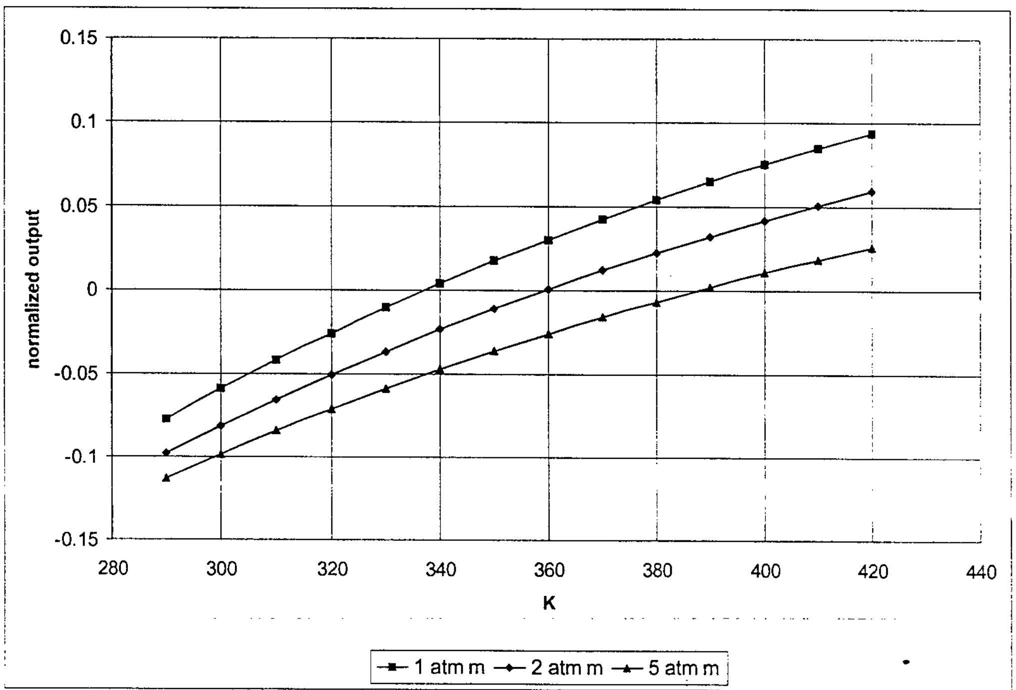

2.2.3 Radiometry

The temperature resolution or NEΔT of the thermographer is extracted from a noise equivalent radiance (NER) calculation. NER for this system is given by

$$NER = \frac{4 \cdot (f/\#)^2 \cdot \sqrt{\Delta f}}{\pi \cdot D^* \cdot \varepsilon \cdot t \cdot \sqrt{A_D}} \qquad (7)$$

where f/# is the telescope f-number (equal to the focal length divided by the primary mirror effective diameter), Δf is the detection bandwidth, D* is the microbolometer detectivity, ε is the target emissivity, t is the radiometric efficiency, and A_D is the detector area. Table 3 lists the relevant system values which will be described in more detail under *Phase I Optical Design*

Table 3: System Values

QUANTITY	VALUE	UNITS
f	114	cm
D_o	25.4	cm
f/#	4.5	unitless
Δf	1	Hz
D*	3×10^8	cm√Hz/W
ε	0.7	unitless
t	0.5	unitless
A_D	0.08	cm^2

Given all of these values, the system NER is 8.636×10^{-7} W/(ster cm^2). The corresponding signal to noise (SNR) for a 310K target is 3730.5. NEΔT is found by normalizing the NER and dividing by the slope of the line depicted in figure 4.

$$NE\Delta T = \frac{\sqrt{2}\cdot NER}{slope\cdot(S_1(310)+S_2(310))} = 0.2K = 200mK \tag{9}$$

The √2 results from the two independent noise sources.

2.2.4 Accuracy

The temperature accuracy of the proposed system will be limited by the NEΔT for the case where a separate calibration module is included with the final package. In the absence of a calibration module, the accuracy is limited by the root-sum-square of all of the system uncertainties.

$$\Delta T = \frac{1}{slope}\cdot\sqrt{\left(\frac{\partial S}{\partial S_1}\cdot\Delta S_1\right)^2 + \left(\frac{\partial S}{\partial S_2}\cdot\Delta S_2\right)^2 + \left(\frac{\partial S}{\partial \tau_1}\cdot\Delta\tau_1\right)^2 + \left(\frac{\partial S}{\partial \tau_2}\cdot\Delta\tau_2\right)^2 + \left(\frac{\partial S}{\partial B}\cdot\Delta B\right)^2} \tag{10}$$

Where ∂S/∂variable are the partial derivative with respect to each variable. ΔS_1 and ΔS_2 are the NERs of each channel, and $\Delta\tau_1$ and $\Delta\tau_2$ are the uncertainties in the relative humidity measurements made to correct for water vapor attenuation. ΔB is the uncertainty in the background radiance calculation. Table 4 lists the values assumed (or calculated with the analytical model) for the accuracy calculation and the resulting systemic uncertainty.

Table 4: Values for Accuracy Calculation

QUANTITY	VALUE	DESCRIPTION
T_{target}	310K	target temperature
ΔS	8.636×10^{-7} W/(ster cm^2)	NER
$S_1(310)$	3.222×10^{-3} W/(ster cm^2)	channel one response
$S_2(310)$	2.693×10^{-3} W/(ster cm^2)	channel two response
$\Delta T_{background}$	0.1K	error in background temp. measurement
$T_{ambient}$	293K	ambient temp.
ΔRH	0.015	error in relative humidity measurement
RH	0.5	relative humidity
ΔP_{wv}	0.0013 atm	error in water vapor concentration calculation*
L	1000 m	pathlength to target
ΔL	1 m	error in pathlength measurement
$t_1=t_2$	0.816	transmission through each filter
Δt	.013	error in transmission calculation**
ΔT_{target}	**2.67K**	**systemic accuracy**

* This error assumes a ±1°C accuracy ambient measurement.

** Δt depends on ΔP_{wv} and ΔL.

2.3 Phase I Optical Design

2.3.1 The Telescope

The Phase I optical system incorporated a 10" f/4.5 Newtonian telescope made by Meade Instruments Corporation (shown in figure 6). The eyepiece is replaced with the breadboard sensor module which is held to the side of the tube using rubber feet and straps. The primary and diagonal mirrors are Grade-A Pyrex®, and the optical tube is a 12.7"×45" long spiral-wound Sonotube. The diagonal support is a 4-vane steel spider.

Figure 6: Phase I Telescope with Sensor Module

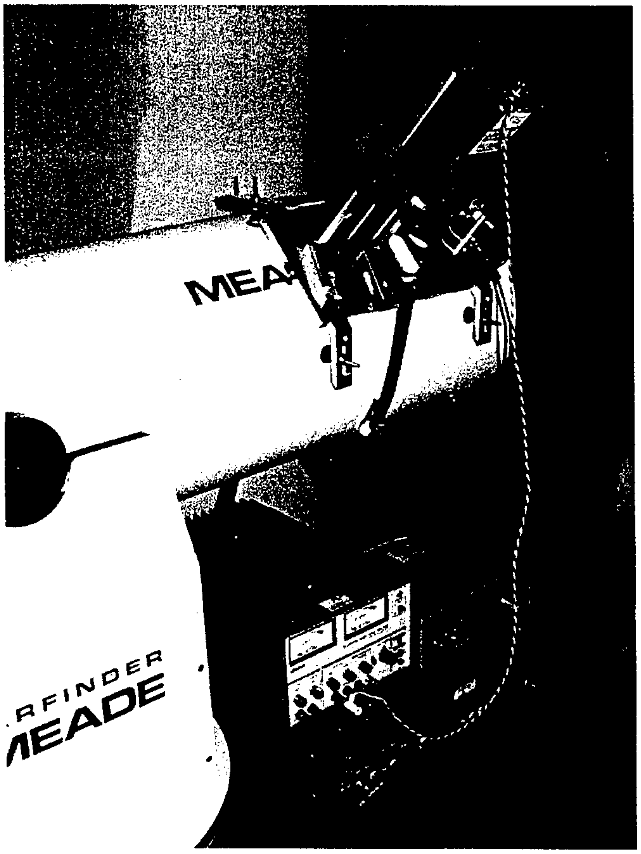

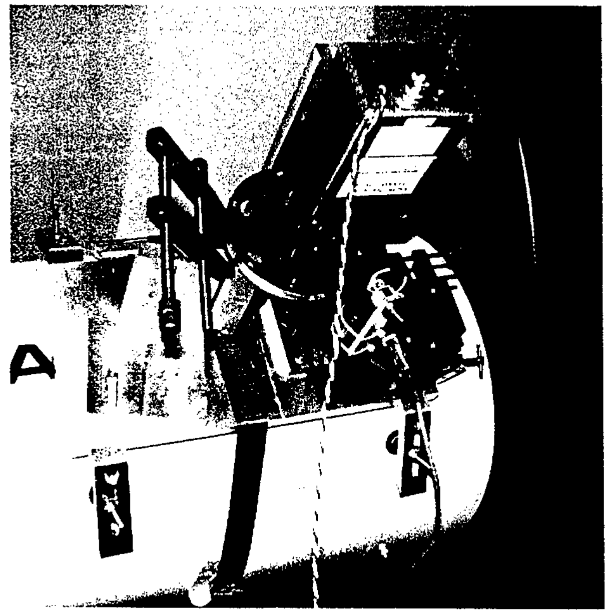

Figure 6: Phase I Telescope with Sensor Module
The Phase I telescope was a 10" f/4.5 Meade Instruments Newtonian telescope. We replaced the eyepiece with the thermographer sensor module, which was held in place with rubber feet and a strap. The primary and diagonal are Grade-A Pyrex®, and the optical tube is a 12.7"×45" long spiral-wound Sonotube. The diagonal support is a 4-vane steel spider.

2.3.2 The Sensor Module

The sensor module is composed of a chopper and the a-Si microbolometer detector with the two IR filters on a filter wheel. The chopper is placed to intercept the focusing exit beam from the telescope. The collected light is focused through a filter and onto the microbolometer. Figure 7 shows the optical model in Zeemax. Note that the design deviates from the original intention of utilizing two microbolometers because of the unavailability of a sufficiently stable reflective chopper. The configuration realized in the Phase I is more representative of the Phase II system which uses a single microbolometer focal plane array (FPA) with alternating filters.

Figure 7: Phase I Optical Design

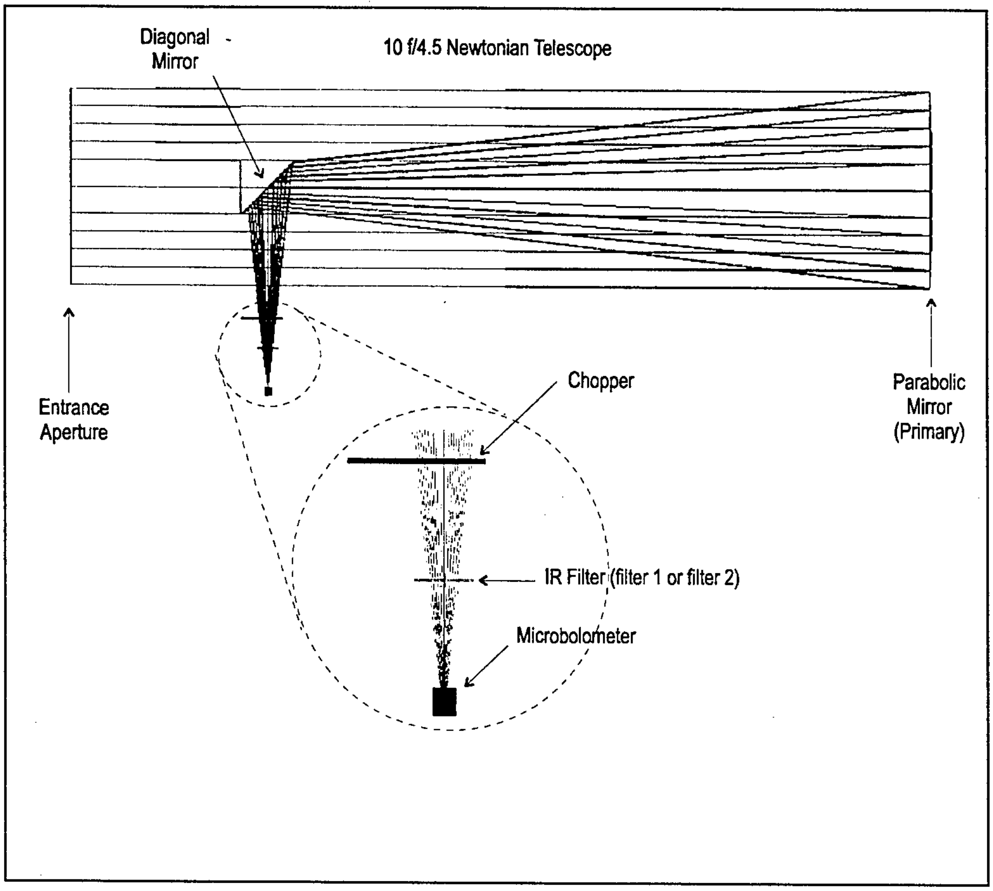

Figure 7: Phase I Optical Design
Shown above is the Zeemax Phase I optical design of the 10" f/4.5 Newtonian telescope with the components comprising the sensor module. The light exiting the telescope is modulated by the chopper before passing through one of the two filters onto the microbolometer. The two filters are mounted onto a filter wheel.

2.3.3 The Microbolometer

The amorphous silicon microbolometer was procured from Raytheon Systems in Dallas, TX. We received spectral response, frequency response, and detectivity data along with the detectors. We verified frequency response and detectivity in house. Figures 8a and b show the spectral and frequency responses respectively. The D* measured in house was within experimental error of the 3×10^8 cm$\sqrt{}$Hz/W measured by Raytheon.

Figure 8a: Microbolometer Spectral Response

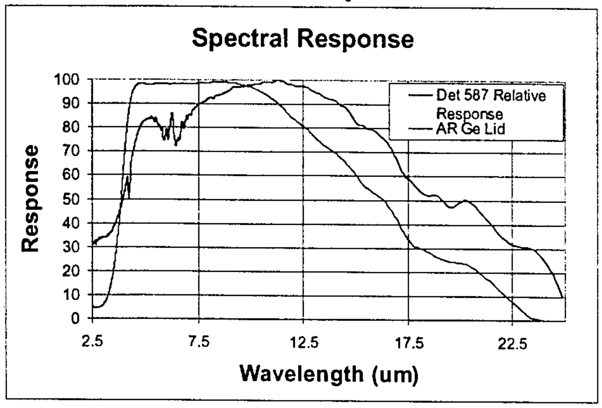

Figure 8b: Microbolometer Frequency Response

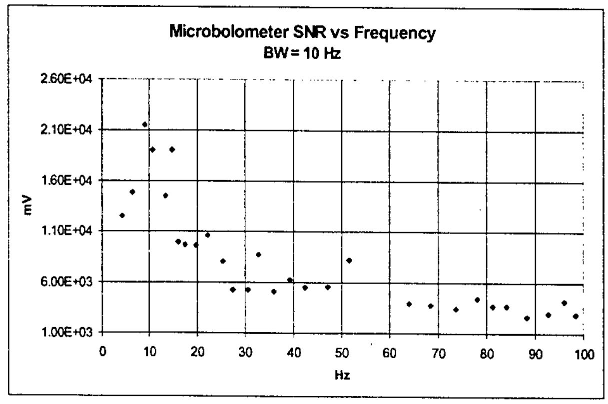

2.4 Phase I Mechanical Design

The Phase I mechanical design consists of the baseplate which straps to the side of the telescope tube and the adjustable mounts for the microbolometer and chopper (figure 9). The microbolometer mount allows for three degrees of adjustment freedom, allowing the target image to be centered and focused onto each microbolometer (realized using slotted through holes).

Figures 9: Phase I Thermographer Mechanical Design

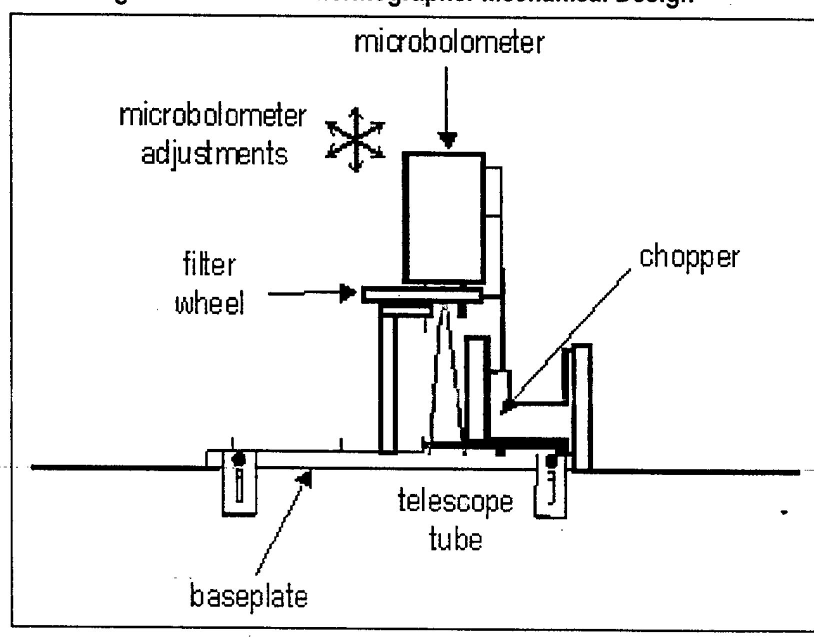

2.5 Phase I Electronics

A synchronous detection scheme using a lock-in amplifier was used to recover the AC signals from the microbolometer. Using the output of the photointerupt on the chopper as the frequency reference, the signal is sampled. The lock-in is an EG&G Princeton Applied Research Model 5110.

The benefit of synchronous detection is that it allows the signal of interest to be measured in a higher frequency, lower 1/f noise region. The general mechanism is that the modulated signals (i.e. the microbolometer outputs) are multiplied by an electric signal of the same frequency (i.e. the chopper reference) and low pass filtered. The result is the DC signal of interest.

Figure 10: Synchronous Detection

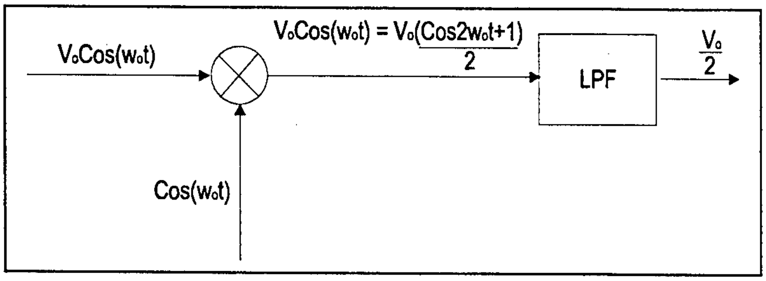

3.0 SYSTEM TESTS

3.1 Performance Evaluation

The following tests comprise the performance evaluation of the Phase I system.

1. System Response

The system response to a controlled blackbody was recorded as a function of temperature. As shown in figure 11, the blackbody target was placed 102 feet from the front end of the telescope; the telescope was aimed and the microbolometer adjusted to the image plane. The blackbody was ramped down from 120 to 20°C, and the signal through each filter was measured in roughly 7° increments. The response curves for the difference, sum, and normalized difference of the two channels were generated for analysis.

Figure 11 System Response Test Set Up

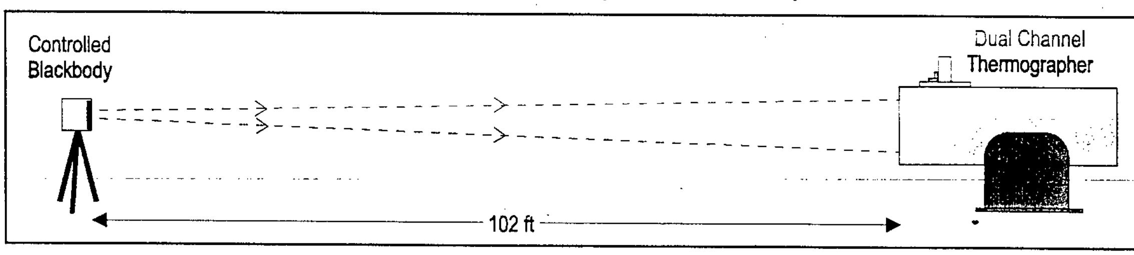

The blackbody used for this measurement was built in house. It is composed of a household iron powered through an Omega temperature controller (Monogram CN76000). A 4.5×4.5×0.375 inch piece of aluminum was affixed to the iron face using thermal grease and thermal epoxy. The aluminum piece was painted with a flat black high-temperature paint. An Omega C01-K cement-on thermocouple was clamped to the front of the aluminum piece with more thermal grease and a metal clamp. The thermocouple provided feedback to the controller, and the temperature could be accurately controlled to better than a degree. Figure 12 shows a photograph of the controlled blackbody. The cardboard baffle was used to shield the blackbody from wind (all data was collected with the blackbody outside).

Figure 12 Controlled Blackbody

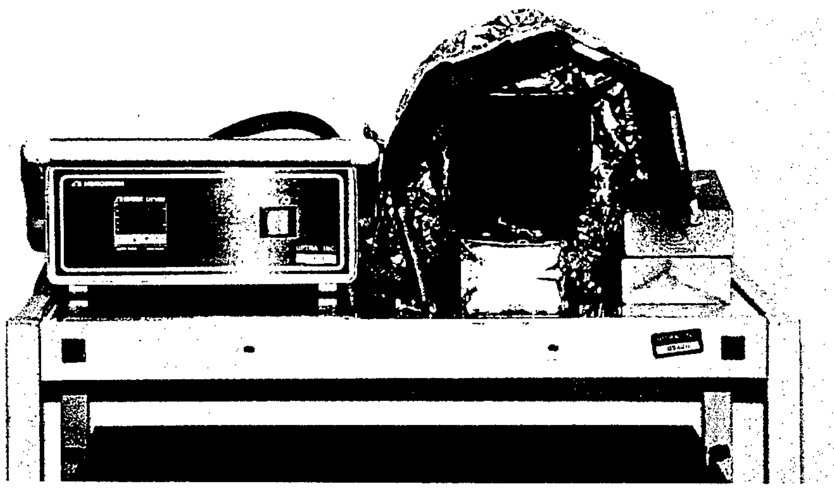

2. NEΔT

Noise equivalent temperature was determined by measuring the local slope of the response curve generated in test 1. The rms noise was determined from the lock-in display; the peak-to-peak was divided by $2\sqrt{2}$. The NEΔT is then given by

$$NE\Delta T = \frac{noise_{rms}}{slope} \tag{11}$$

for the sum and difference curves and by

$$NE\Delta T = \frac{\sqrt{2} \cdot noise_{rms}}{slope \cdot (S_1(T) + S_2(T))} \tag{12}$$

for the normalized difference. The $\sqrt{2}$ is due to the two independent noise sources.

3. Accuracy

Accuracy was evaluated by returning the blackbody to designated temperatures within the range and utilizing the curves generated in test 1 to assess the accuracy. This is also a repeatability test. Again, the three response curves were evaluated.

4. Field of View

The field of view was determined by measuring the image size of a target of known size as well as the standoff to the target. The image size was determined by comparing it to a series of square templates of 0.005 inch increments. Magnification is determined according to

$$M = \frac{image}{object} \tag{13}$$

The target size accepted by the 2 mm microbolometer is then given by

$$\text{target} = \frac{2\text{mm}}{M} \tag{14}$$

Given the standoff distance, the field of view is then

$$FOV = 2 \cdot \tan^{-1}\left(\frac{\text{target}}{\text{standoff}}\right) \tag{15}$$

5. Skin Temperature Measurement

The skin temperature of a subject's face was measured with the thermographer using the three calibration curves (and the same 102-foot standoff).

3.2 Results

1. System Response

Figures 13a through c show the system response to the target temperature for the difference, sum, and normalized difference between the two channels respectively.

Figure 13a: Difference Response

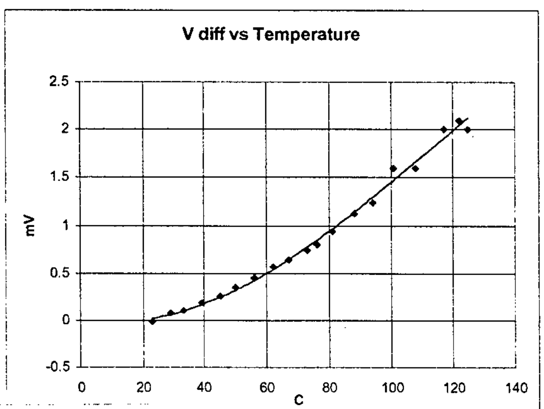

Figure 13a: Sum Response

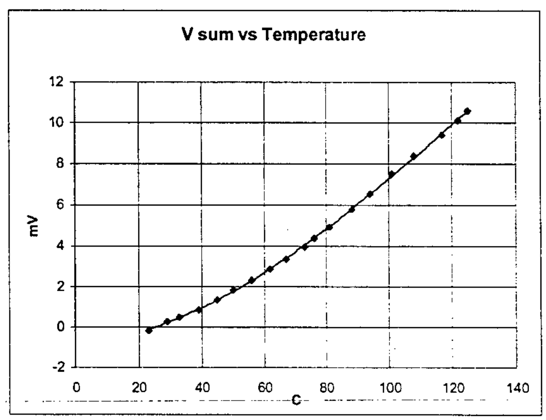

Figure 13c: Normalized Difference Response

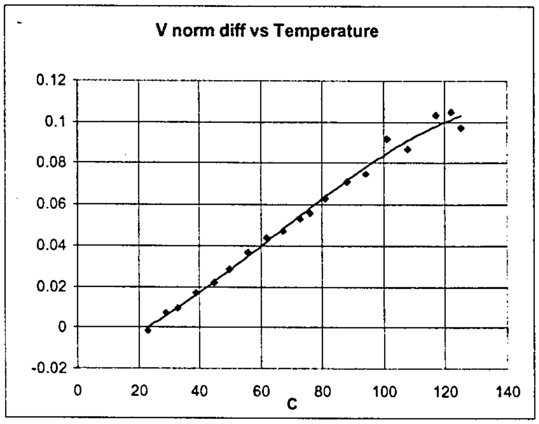

Figures 14a through c show the quasi-linear responses over the low-temperature region (linear equations given):

Figure 14a: Difference Response (low temperature)

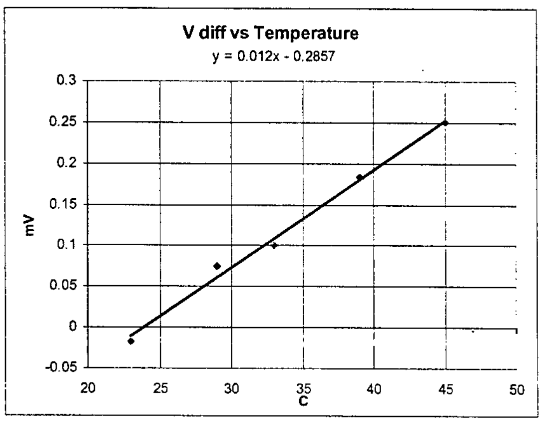

Figure 14a: Sum Response (low temperature)

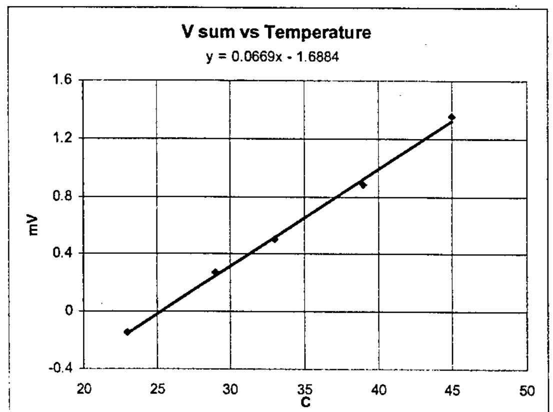

Figure 14a: Normalized Difference Response (low temperature)

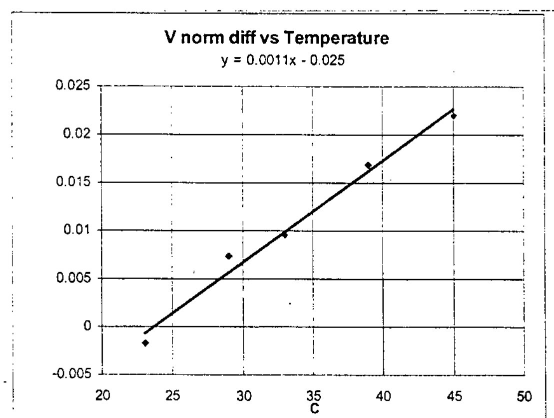

2. NEΔT

The lock-in noise was determined to be 5 μV peak to peak or 1.77μV rms. Table 5 lists the NEΔTs for each response curve at 39°C. Note that the NEΔT for the normalized difference decreases at the target temperature increases.

Table 5: NEΔT

RESPONSE CURVE	NEΔT
Difference	0.2°C
Sum	0.036°C
Normalized Difference	2.4°C

3. Accuracy

Table 6 lists a short series of blackbody temperatures (as measuring by the thermocouple) and the corresponding difference, sum, and normalized difference values.

Table 6: Thermographer Accuracy

T_{TC}	SUM	DIFFERENCE	NORMALIZED DIFFERENCE
86°C	93°C	85.75°C	82.75°C
56°C	61°C	56.75°C	55.5°C
48°C	52.25°C	48.5°C	47.3°C
41°C	44°C	43.5°C	42.75°C

On average, the difference calculation resulted in the most accurate temperature measurement with an average error of 1°C. The sum calculation exhibited an average error of 4.9°C, and the normalized difference an average error of 1.5°C (but is independent of ε).

4. Field of View

The image size for a 4.5 inch target was measured to be 0.155 inches. The magnification is, thus, 0.0344. The target size accepted by the 0.0788 inch microbolometer is 2.28 inches according to equation 14. The corresponding field of view is 0.103°.

5. Skin Temperature Measurement

A skin temperature measurement was made on a human subject's face at the 102 foot standoff. The measured temperatures were 38°C using the sum curve, 32°C using the difference curve, and 30.9°C using the normalized difference curve. Based on our short accuracy study, we believe the subject's face temperature to be 32°C ±1°C.

3.3 Comments on the Data

We have substantiated that a surface temperature measurement based on taking the difference between two near-by spectral channels is a viable method. One very important benefit of this method is that taking the difference automatically subtracts out almost all background radiation which may contaminate the measurement if not corrected. The sum measurement (which is analogous to using a single channel) suffers from poor repeatability when the background conditions change (e.g. the building heats up). This problem may be solved by including a background temperature measurement of the sensor module each time the thermographer is used. Another option would be to design the optical system such that *only* the light exiting the telescope (i.e. the target radiance) is modulated by the chopper; the lock-in detection technique will *only* measure the signal value modulated at the chopper frequency. The normalized difference method seems to provide adequate accuracy, though it also includes a background factor in the denominator. The normalized difference has the potential, however, to factor out the emissivity of the target given that the background has been subtracted. The NEΔT is highest for the sum and lowest for the normalized difference on account of varying discriminant signals.

Overall, the measured system performance agrees with the analytical model given the uncertainty of the background compensation.

4.0 CALIBRATION ROUTINE

Section 2.2 *System Analysis* presents the measured radiance values of each IR channel, incorporating the IR filter profiles, target emissivity and spectral radiance, and water vapor transmission of the measurement path. The actual electrical signal resulting for each radiance measurement, however, contains an additional responsivity term which is a function of the product of the microbolometer's spectral response (figure 8a) and its responsivity (in volts/watt). In addition, each expression also contains a variable gain factor, A, which is proportional to the difference in temperature between the chopper and the target. The following equations give the complete expressions for each channel and denote the water vapor concentration-pathlength dependence.

$$S_1(T,CL) = \int_\lambda A \cdot I_1(\lambda) \cdot \varepsilon \cdot N(\lambda,T) \cdot \tau_{wv}(\lambda,CL) \cdot R_{\mu b}(\lambda)\, d\lambda \qquad (16a)$$

$$S_2(T,CL) = \int_\lambda A \cdot I_2(\lambda) \cdot \varepsilon \cdot N(\lambda,T) \cdot \tau_{wv}(\lambda,CL) \cdot R_{\mu b}(\lambda)\, d\lambda \qquad (16b)$$

$R_{\mu b}$ is given by

$$R_{\mu b} = R(\lambda) \cdot R_o \qquad (17)$$

where $R(\lambda)$ is the spectral response of the microbolometer (figure 8a) and R_o is its responsivity (in volts/watt).

The calibration routine takes all of the above vales into account (either by measuring them as part of the thermographer's operation mode or by treating them as constant values). Figure 15 shows a flow diagram of the calibrated operation. Blue denotes hardware, pink denotes software or algorithms, and yellow denotes a measured quantity.

Figure 15: Block Diagram of Calibration

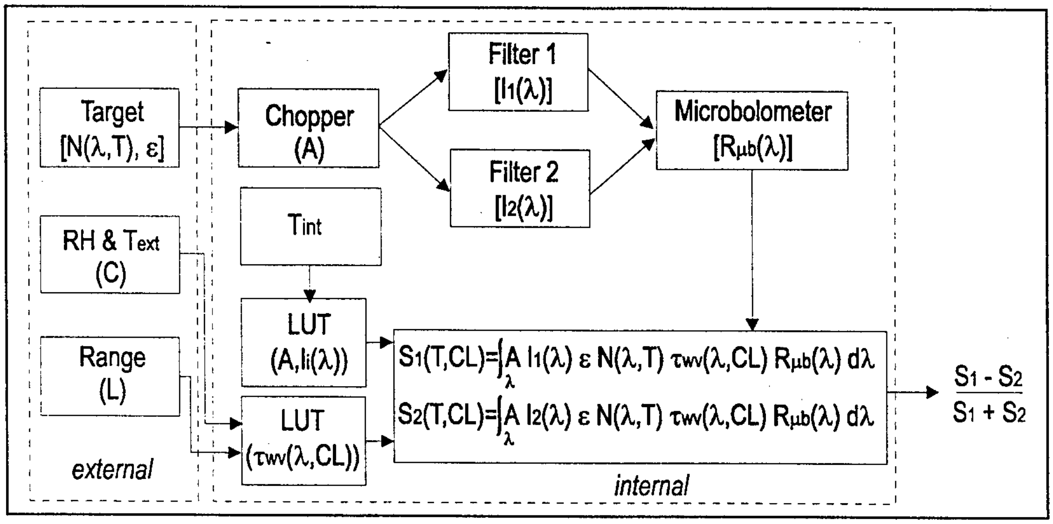

As explained in the Phase II proposal, we intend to correct for water vapor in the measurement path by making an independent relative humidity and an ambient temperature measurement to determine water vapor concentration and a range measurement using the telescope mirror position when the target is in focus to determine the pathlength. In addition, an internal temperature measurement will be made and used to correct for a slight temperature-dependent shift in the center of the passband of the filters as well as for a gain factor proportional to the chopper temperature. All of these factors are applied to the resulting signals for each channel and corrected for to determine the actual response of the system. The following steps outline how the calibration works.

1.) Input voltage proportional to target temperature (i.e. microbolometer output)
2.) Measure relative humidity and ambient temperature
    2a.) Input values to waver vapor transmission look-up table
3.) Measure range to target
    3a.) Input value to water vapor transmission look-up table
    3b.) Output water vapor transmission
4.) Measure internal temperature
    4a.) Input value to gain / filter shift look-up table
    4b.) Output gain and shifted filter profiles
5.) Input water vapor transmission, gain, and shifted filter profiles to digital signal processor (DSP) and calculate resulting offsets and change in gain *due to water vapor and internal temperature changes*
    5a.) Correct for offsets and gain
6.) Calculate normalized difference of corrected signals and output as measured target temperature.

These corrections will execute as part of normal operation. The Phase II work will determine whether additional calibration (i.e. a fielded calibrated blackbody) is necessary.

5.0 SYSTEM COST MODEL

The final Phase I objective was to formulate a system cost model to predict the price of a final system in production quantities. The following table gives this cost model for the system described in our Phase II proposal in two variations: with and without imaging capabilities. The latter option provides a lower-cost alternative which may be preferable in some instances.

Table 7: Material Cost Model

IMAGING OPTION			NON-IMAGING OPTION		
COMPONENT	**SOURCE**	**COST**	**COMPONENT**	**SOURCE**	**COST**
VO_x FPA (with chopper/shutter)	ISI	$11,500	Single Channel a-Si Microbol.	Raytheon	$100
IR Filters (x2)	OCLI	$240	IR Filters (x2)	OCLI	$240
Sensor Module Housing	Engineering Estimate	$500	Sensor Module Housing	Engineering Estimate	$500
Sensor Module Optical Mounts	Engineering Estimate	$1000	Sensor Module Optical Mounts	Engineering Estimate	$1000
16" Primary Telescope Mirror	Edmund Scientific	$4155	16" Primary Telescope Mirror	Edmund Scientific	$4155
4" Secondary Telescope Mirror	Engineering Estimate	$1000	4" Secondary Telescope Mirror	Engineering Estimate	$1000
Thermocouple	McMaster-Carr	$40	Temperature Sensors (x2)	McMaster-Carr	$40
Hygrometer / Thermometer	VWR Scientific	$175	Hygrometer / Thermometer	VWR Scientific	$175
Tripod	Engineering Estimate	$800	Tripod	Engineering Estimate	$800
Laptop PC with PCI Slots	Field Works Inc.	$8395	Embedded CPU	EMJ Embedded	$725
Frame Grabber	Imaging Tech	$1250	Liquid Crystal Display	NEC	$250
Cable	Imaging Tech	$285	Singe Channel 16-bit A/D	Analog Devices	$52
			Quad 8-bit A/D	Maxim	$10
			Optical Chopper with DC Motor	Thor Labs/ McMaster-Carr	$100
Total:		**$29,340**			**$9,147**

Table 8: Labor Cost Model

TASK	HOURS	COST
Assemble Telescope Mirrors	1	120
Assemble and Align Sensor Module	1.5	180
Assemble Environmental Sensors	.25	30
Integrate and Test Electronics	2	240
Test System	~~1~~	~~120~~
Total	5.75	**$690**

This cost model demonstrates a significant cost benefit for selecting the non-imaging option, not only due to the high price of the focal plane array but also the additional requirements of a laptop with PIC slots for the frame grabber card. The non-imaging option requires some simple A/D's and an embedded processor with an LCD to display temperature, system status, etc. It is notable, however, that the IR FPA industry is currently working towards a significant cost reduction; the target price will ultimately be less than $1000. In addition, the price of the laptop with PCI slots will undoubtedly come down as is the PC trend. The system cost with these considerations can be as low as $11,945 assuming a typically priced laptop of $1500. These developments will ultimately make the imaging option competitive with the non-imaging option in terms of price.

6.0 PHASE I REVIEW

6.1 Review of Phase I Test Results

The Phase I test results are summarized in table 9 where they are also compared to the predicted value for the *normalized difference measurement only.*

Table 9: Phase I Predicted and Measured Values

QUANTITY	PREDICTED	MEASURED
Slope of Response	1.033×10^{-3}/°C	1.1×10^{-3}/°C
NEΔT	0.2°C	2.4°C
Accuracy	Not Predicted*	1.5°C
FOV	0.1005°	0.103°C
Skin Temperature	25-35°C	30.9°C

* Accuracy for no atmospheric or background correction was not predicted. This number will ultimately be limited by the NEΔT of the system.

Comments on the agreement of the predicted and measured values are given below for each quantity.

Slope of Response

The slope of the response originally predicted by the MathCAD model (in units of nepers/°C) did not take into account the effects of background radiation or the spectral response of the microbolometer. The measured value was therefore adjusted for background. In general, they agree well considering the known sources of error. The effects of background radiation will be corrected in the Phase II system – most likely by designing the optical system such that only the exit aperture of the telescope is modulated by the chopper. The synchronous detection will only lock-in to the modulated radiance from the target in this case.

NEΔT

The NEΔT measured was an order of magnitude worse than predicted by the model. While the measured value will still be useful for this application, a reconciliation between the measured and predicted values must be made to verify the model.

We believe that the root of the discrepancy is again the effects of background radiation. One problem area was that when the target temperature approached that of the chopper, we notice what seemed like an elevated level of system noise as the amplitude of the signal approached zero. What happens here is that the phase of the AC signal is flipping from 0 to 180° (figure 16). The effective signal to noise going into the lock-in is small in comparison to *either* high or low target temperatures. One solution to this problem is to implement a reflectively cooled chopper such as was discussed in the 4th progress report (figure 17).

Figure 16: Temperature-Dependent Phase

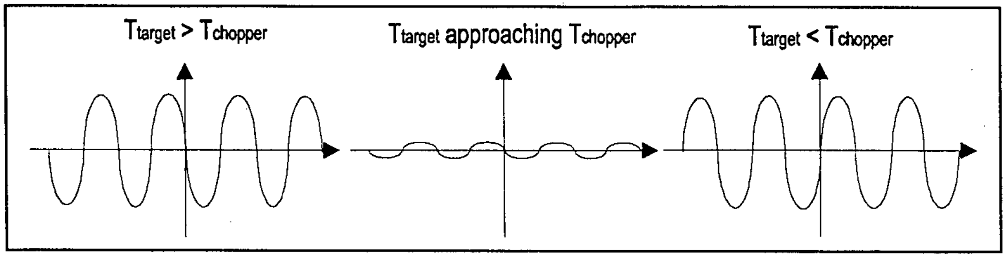

Figure 17: Reflectively-Cooling the Chopper

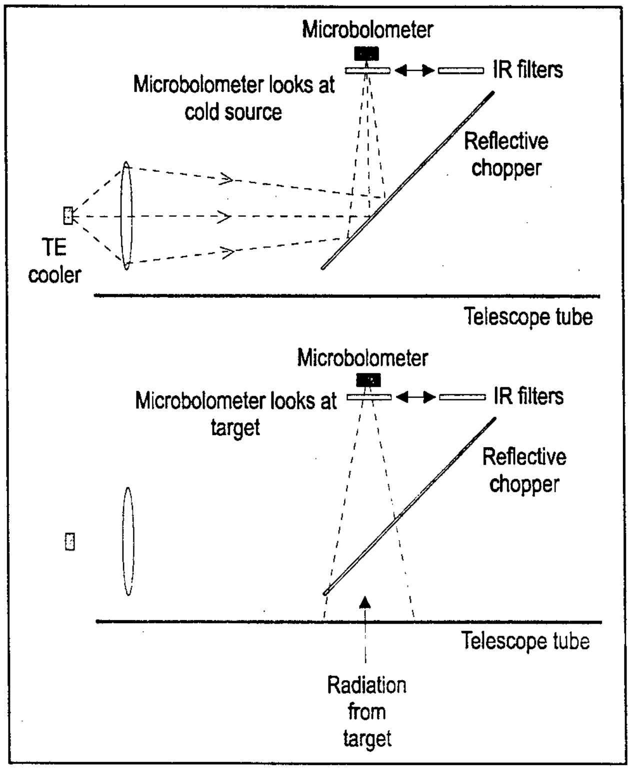

An additional point to make is that, because of the extremely low bandwidth of the microbolometer (figure 8b), we operated the chopper (and synchronous detection) at around 10 Hz, which does not offer much benefit in terms of operating at a lower 1/f-nosie region. We may want to consider operating at a higher bandwidth for the Phase II system (which will be using the focal plane array which is operable at higher frequencies).

Accuracy

The repeatability measurement we made yielded an average temperature error of 1.5°C for the normalized difference measurement, which actually exceeds the measured NEΔT. As the number of data points taken during this measurement was small, we would recommend additional study of this quantity during the Phase II.

FOV

The measured field of view was extremely close to the design quantity. This agreement simply attests to our ability to make an accurate optical design.

Skin Temperature

Our skin temperature measured value was perfectly reasonable given the ambient conditions when the measurement was made.

6.2 Atmospheric Attenuation

Atmospheric attenuation is the first of four areas of concern we signed on to conceptually address in meeting the second technical objective of the Phase I Continuity. This issue, however, has already been addressed in the *Calibration Routine* section.

To reiterate, we intend to execute external relative humidity and temperature measurements to calculate the concentration of water vapor in the ambient air according to

$$P_{wv} = RH \cdot P_{sat}(T_{amb}) \tag{18}$$

where P_{wv} is the water vapor partial pressure, RH is the relative humidity, and $P_{sat}(T_{amb})$ is the saturated partial pressure of water at the ambient temperature. RH and T_{amb} are measured by independent sensors and input to a water vapor transmission look-up table (LUT). In addition, the measurement path from the sensor to the target is determined by measuring the position of the telescope mirror while the target is in focus. This pathlength is also input to the LUT. The LUT then calculates and outputs the water vapor transmission profile to a DSP which corrects for the offset in the temperature measurement due to water vapor in the path.

6.3 Calibration

This issue was also addressed in a previous section. It is brought up again here to offer that we will determine during the Phase II whether additional field calibration is necessary based on repeatability studies. This field calibration module would consist of a calibrated blackbody and dedicated optics as shown conceptually below.

Figure 18: Concept of Calibration Module

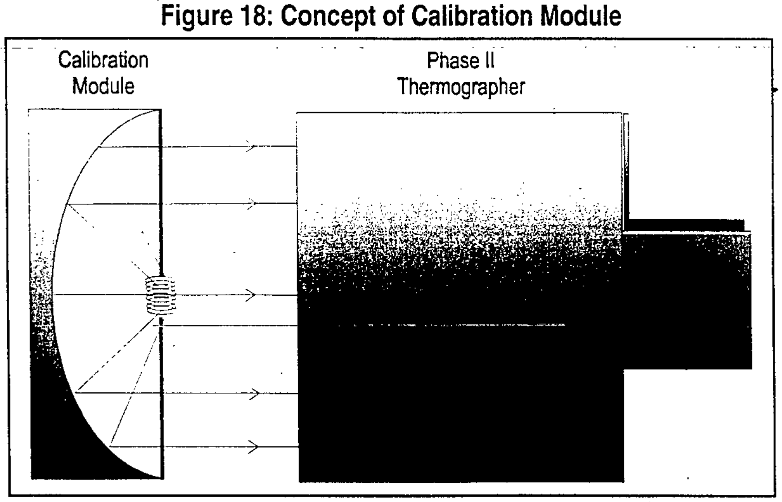

6.4 Temperature Logging

As described in detail in the Phase II proposal, we intend to incorporate a microbolometer focal plane array with a PC interface in the Phase II system. The system will adopt a user-friendly graphical user interface (GUI) which allows the operator to view, acquire, and store images via a frame grabber installed in a ruggedized laptop PC with PCI slots. The PC also accepts the external RH and temperature measurements as well as the internal temperature measurement for use in the correction algorithms. The FPA interface and software conceptual designs are presented in detail in section 7, *Phase II Conceptual Design.*

6.5 Aiming

We intend to develop a user-selected target field of view as part of the GUI for the Phase II system. The system will allow the user to adjust the size of a central portion of the full field of view within which the mean absolute temperature can be measured (through coadding pixels in the FPA). This allows for enhanced NEΔT at shorter standoff distances with respect to the target. The boundary of this selected target field of view will be displayed on the laptop screen as a black and white square, as shown in figure 19. At the bottom of the laptop display there will be a digital readout of the central target temperature and related data.

Figure 19: Variable Field of View

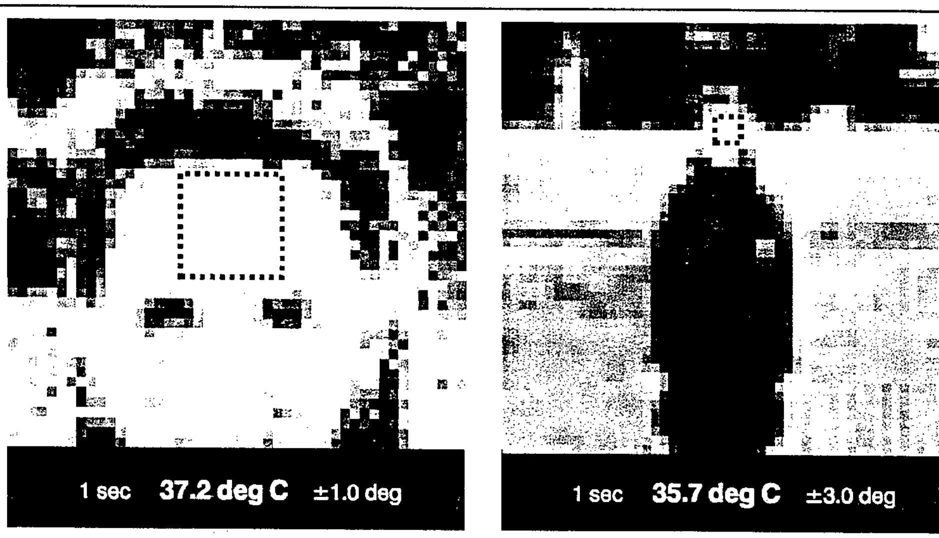

Figure 19: Variable Field of View

The two figures above show portions of the Thermographer image display for targets at ranges of 100 meters and 500 meters In both cases the areas shown are 50 x 50 pixels (out of a full field-of-view of 160 x 120 pixels). The black & white dashed squares show the user-selected FOV within which the temperature measurement is made. The larger the square, the higher the resolution of the temperature measurement. The variable FOV allows the user to make intelligent trade-offs between angular resolution in the image, and temperature resolution in the measurement. As illustrated above, the displayed measurement shows both the user-selected integration time and the temperature accuracy.

7.0 PHASE II CONCEPTUAL DESIGN

7.1 Conceptual Design Introduction

The following is the conceptual design developed for the Phase II proposal. The opto-mechanical design as well as detector choice supports an NEΔT of the normalized difference signal of 0.8 K for an f/2.8 system (corresponding to a 25 cm spot at a 500 m standoff). The radiometry is presented in detail in the Phase II proposal and will not be reiterated here as part of the Conceptual Design.

7.2 System Conceptual Design

The fundamental idea is to provide a thermal imaging capability combined with an accurate temperature measurement for a selected area in the center of the field of view. The accurate temperature measurement is based on the normalized difference between signals collected through two separate bandpass filters (8 to 11μm and 9.5 to 12.5μm). This temperature measurement is independent of the target emissivity and provides good temperature sensitivity for a target area equal to that of a human face.

The proposed Phase II system design includes the following features:

1. 16-inch diameter Cassegrain telescope (1-meter focal length; effective f/2.8)
2. Overall size $\approx 18'' \times 18'' \times 18''$
3. Microbolometer Focal Plane Array (FPA) detector; 160×120 pixels, each 50μm square
4. User-selected central image area within which the mean absolute target temperature is calculated & displayed
5. NEΔT (noise-equivalent temperature difference) $\approx 0.5°$C for the image; NEΔT for absolute temperature measurement depends on size of selected image area (NEΔT $\approx 0.8°$C for a 100 pixel image area and target emissivity of 1)
6. Ruggedized laptop PC with FPA interface showing or including:
    a. The IR image (sum of the two channels)
    b. The user-selected area within which absolute temperature is measured
    c. Digital display of the target temperature (normalized difference of the two channels)
    d. Digital displays of the measurement duration, estimated accuracy, and approximate range (based on focus setting)
    e. Automatic correction for atmospheric attenuation and background radiation
    f. Data and image logging capabilities
7. Battery powered with provisions for external AC or DC power

Figure 20 shows a block diagram of the proposed system.

Figure 20: Phase II System Block Diagram

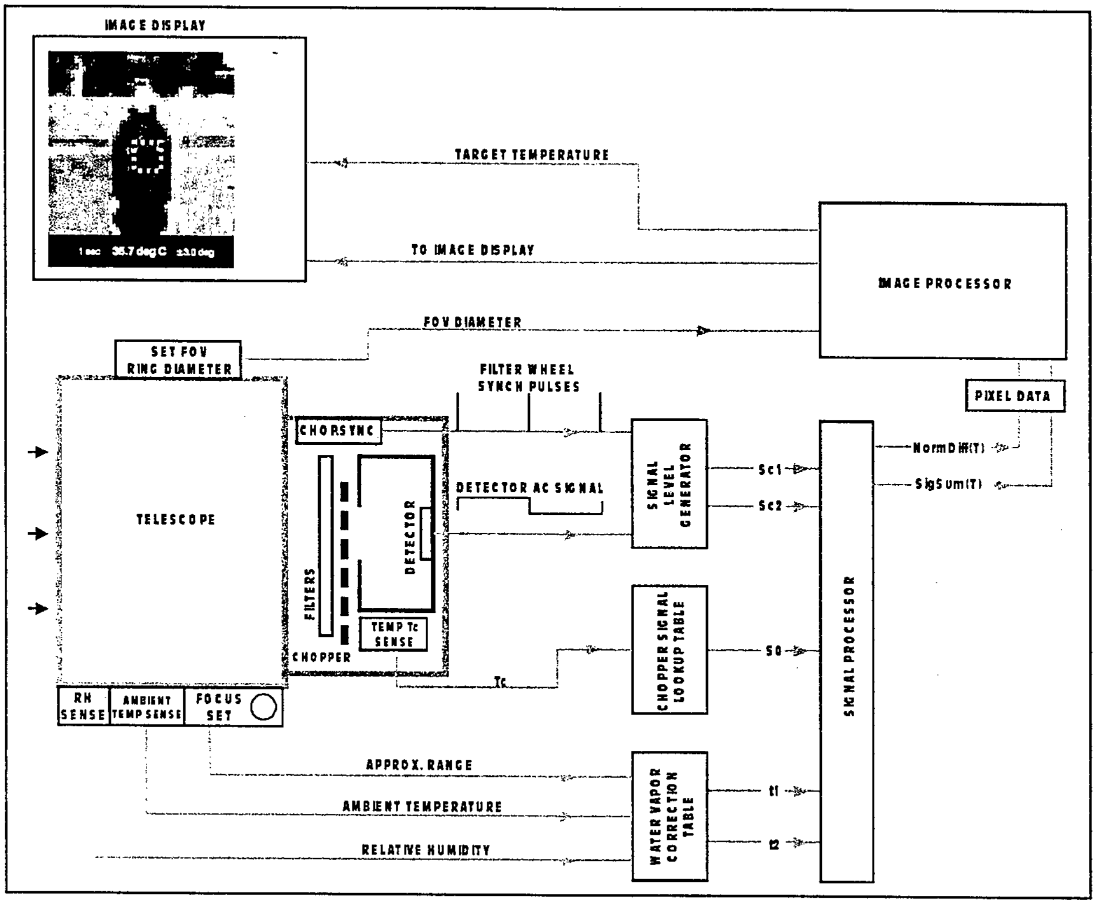

Figure 20: Phase II System Block Diagram

This block diagram illustrates how the detector signals and the signals from the other sensors are collected and processed to produce a temperature value (based on the normalized detector signal difference) for the selected field-of-view, and a thermal image (based on the sum of the detector signals). Range, temperature, and humidity data are used to correct for water vapor absorption and a measurement of the chopper blade temperature is used to properly interpret the chopped detector signals. The user-selected field-of-view is used to determine the spatial averaging that is employed in the target temperature measurement.

7.3 Opto-Mechanical Conceptual Design

The optical design of the system was carried out using the Zeemax Optical Design software package. This software allows full control of system optimization, and can synthesize aberrated images from input bitmaps. It can also generate CAD files showing optical elements and rays paths; these files can be imported into mechanical design CAD software to allow the mechanical hardware to be designed around the actual optical elements and light paths.

The table below shows the preliminary design, and figure 21 illustrates the proposed telescope configuration.

Table 10: Zeemax Optical Design of Cassegrain Telescope

Lens Data Editor: Config 1/4

Edit Solves Options Help

Surf	Type	Comment	Radius	Thickness		Glass	Semi-Diameter		Conic	
OBJ	Standard		Infinity	100000.000000			872.686779		0.000000	
STO*	Standard		Infinity	250.000000			200.000000		0.000000	
2*	Standard	PRIMARY MIRROR	-725.000000	-250.000000		MIRROR	150.000000	U	-1.180006	V
3	Coord Break	FOCUS ADJUSTMENT		31.294729	V	-	0.000000			
4*	Standard	SECONDARY MIRROR	-455.620288	400.000000		MIRROR	55.000000	U	-6.418962	V
IMA	Standard	IMAGE	Infinity				8.809128		0.000000	

As shown in figure 21, the chopper is located so that it chops only light coming from the target (plus the small amount of background radiation from the central obscuration of the secondary mirror); all of the radiation from the baffle surrounding the detector, and from the filter wheel, is un-chopped and therefore not present in the AC signal at the detector. The design of the telescope was optimized for image quality at ranges of 100m, 200m, 500m, and 1000m.

As with all Cassegrain telescopes there is a central obscuration; in this case the secondary mirror obscures approximately 18% of the primary aperture, reducing the effective f/no. from f/2.5 to ≈f/2.8. Should it prove necessary to reduce the overall size of the telescope, the design can easily be scaled down to a 12-inch or 10-inch diameter (at the expense of an increased NEΔT).

The system's field-of-view, defined by the detector array area (8mm $\times$ 6mm) and by the focal length of the telescope (1000mm), is 0.46° $\times$ 0.34°. If desired, this could be doubled without any radiometric penalty by using a germanium field lens and 0.5$\times$ relay lens in the focal plane of the telescope, as shown below.

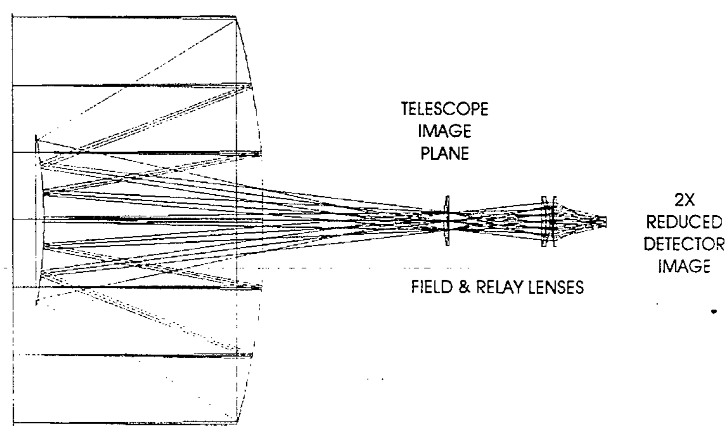

Figure 21: Cassegrain Telescope Layout

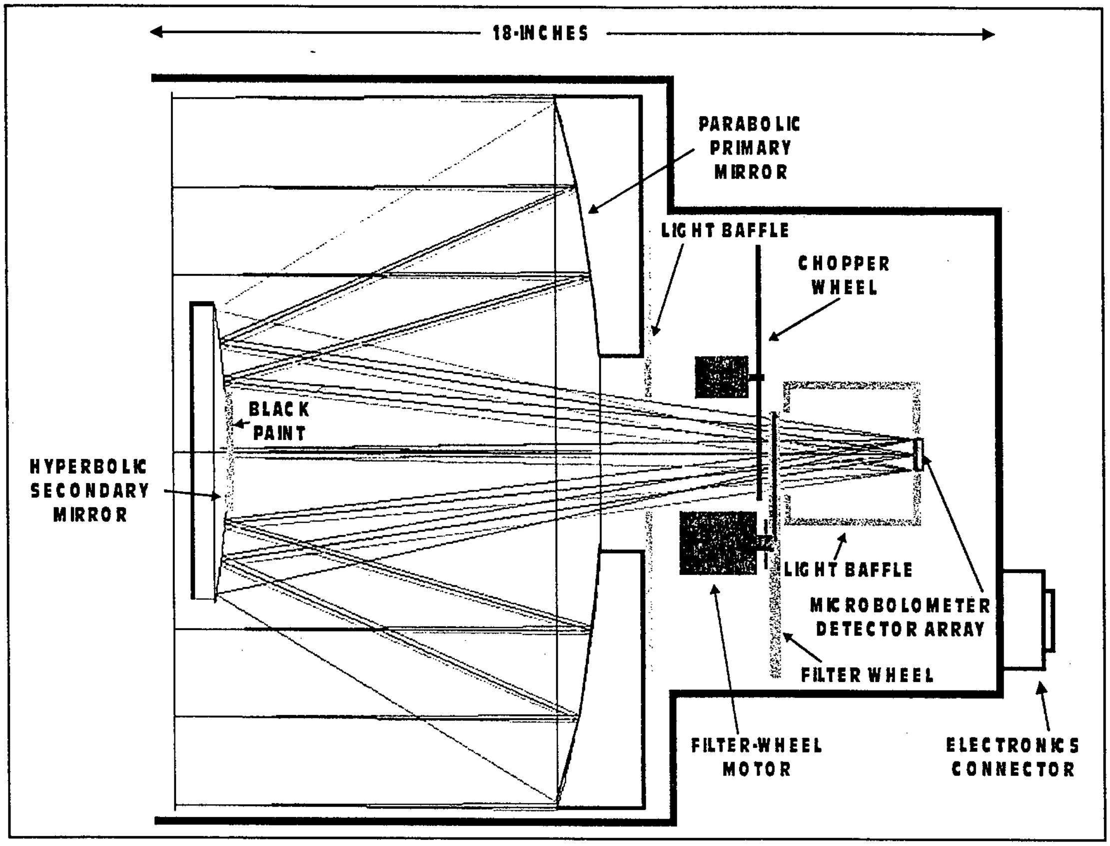

Figure 21 Cassegrain Telescope Layout

This shows the Cassegrain telescope system drawn approximately to scale. The microbolometer detector array (16mm x 12mm) is in the image plane of the telescope. The heavy violet lines represent baffles that are made of aluminum (high thermal conductivity) and painted black. Their purpose is to define the background radiation seen by the detector in a manner that can be characterized by an automated temperature measurement using a thermistor array. The filter wheel allows the detector image to be alternately filtered by the pair of bandpass filters, generating the signal from which the target temperature can be inferred.

The telescope has been designed for optimal imagery over a 1.2-degree field-of-view, and for ranges of from 100 meters to 1 kilometer. The primary mirror is very close to a parabolic, and the secondary is hyperbolic. The baffles have been arranged so that the signal radiation is chopped, while the background radiation (i.e. radiation arriving from outside the field-of-view) is not chopped.

7.4 Electronics Conceptual Design

The electronics design is detailed in Figure 22.

Figure 22: Thermographer Interface Block Diagram

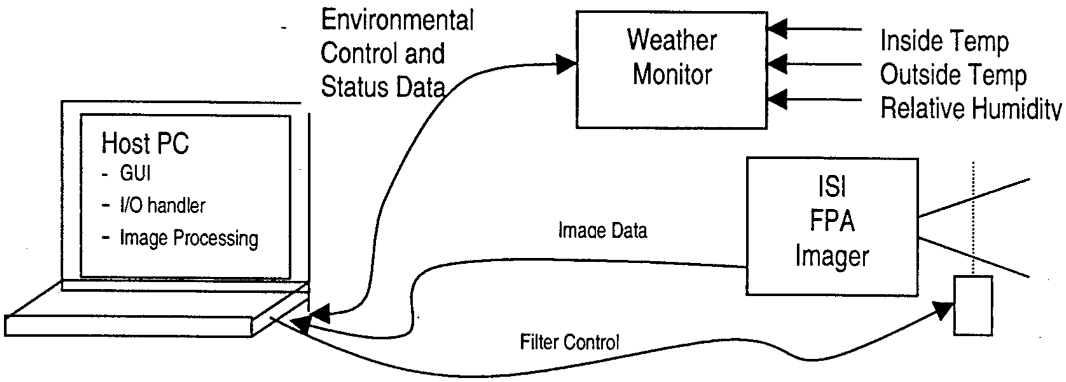

Each subparagraph below describes each of the interfaces shown in Figure 22.

7.4.1 Environmental Control and Status Data

The Environmental Control and Status interface is used to accept inside (sensor module) temperature and outside temperature and humidity information from the weather monitoring subsystem. The interface protocol will be via a standard RS232 serial port on the host PC. This data can be configured to be available at any rate or only on a status request from the host PC.

7.4.2 Image Data

The Image Data interface is used to accept image data from the Imaging Solutions Inc. (ISI) Focal Plane Array (FPA) imaging subsystem. This data will consist of a 160 x 120 pixel array updated at a 15 Hz rate. The interface protocol will be a standard RS422 differential serial port. A complete pixel will be transmitted using 14 bits (or 28 differential) along with three timing and control signal: PCLK (pixel clock), FEN (new frame enable), and LEN (new line enable).

Resident in the host PC is a PCI bus frame grabber board from Imaging Technologies Inc utilized to ease acquisition of image data from the ISI FPA via the RS422. This frame grabber board transfers image data directly to PC memory with 0% load on the host CPU enabling more host processor bandwidth for image processing. Image collection software is available from Imaging Technologies, Inc. for creating custom applications.

7.4.3 Filter Control

The Filter Data interface is used to command the IR filter selection. This will be a single bit command line using a standard RS232 serial port protocol on the host PC. Standard operation will have the filters alternating at roughly 2 Hz.

7.5 Software Conceptual Design

Software for the dual channel remote thermographer will be required to perform the following functions:

- Initialization processing (initialize all internal variables, data constants, I/O communications structures, interrupt handlers, etc; establish and verify all interfaces shown in Figure 22; and initialize the GUI display)
- Accept image data from the ISI FPA imager at a 15Hz rate via the Image Data interface
- Accept environmental data (temperatures and humidity) from the weather monitor via the Environmental Control and Status interface.
- Allow the user to select test control parameters such as IR passband filter selection, filename selection for image data storage, number of image frames to collect, etc)
- Allow user selection of a Region Of Interest (ROI) in the collected image for temperature calculations
- Perform image processing which may include:
    - Image correction
    - Contrast enhancement
    - Atmospheric and background look up table (LUT) processing
    - Temperature calculations on the ROI
    - Filtering
    - Noise calculations
    - Superpixel calculations
    - Decimation
- Display of raw or processed images
- Display of all status data (calculated temperatures, environmental status, etc)
- Perform fault detection of possible error conditions to maintain the integrity of the system/software. The user will be notified via error dialog screens of any possible error conditions.
- Allow processing of previously collected data stored on the PC's hard drive (data collected days or weeks ago may be re-processed or replayed through the system)

7.5.1 Software Interfaces

The software for the dual channel remote thermographer program will consist of three components and various software interfaces shown in Figure 23 and described in the following subsections.

Figure 23: Software Data Flow Diagram

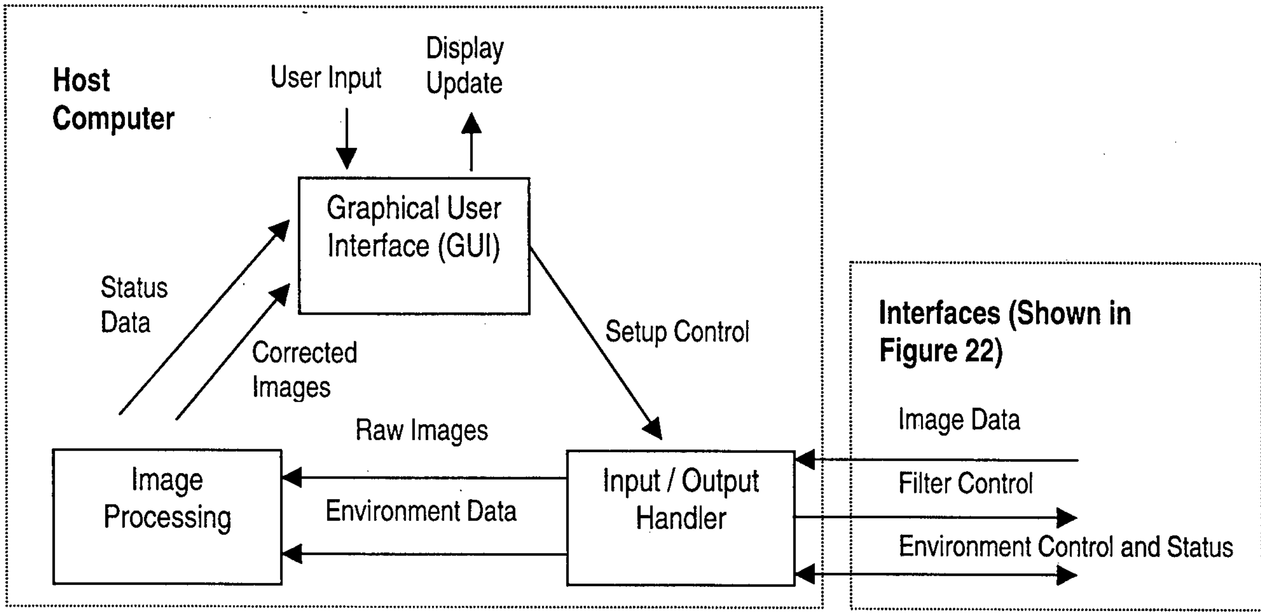

7.5.2 Graphical User Interface

The primary software component of the dual channel remote thermographer is the Graphical User Interface (GUI) resident in the host PC operating under Windows 98 control. The GUI is a user-friendly interface to handle all user input requests and display updates. A template for development of the GUI is shown in Figure 24 and consists of three main areas:

- User Control Input Area
    - Setup control via Filter selection
    - File name selection (File name to store or retrieve image data)
    - Pushbutton control input (Start collection of image data or retrieve previously collected image data from the selected file)
- Image Display Area
    - Displays a contrast enhanced image currently being collected or from a file
- System Status Area
    - Environmental status (Inside and Outside Temperatures, Humidity, etc)
    - Selected region of interest pixel sizes
    - Region of interest temperature calculation
    - Other system status information

Figure 24: Graphical User Interface

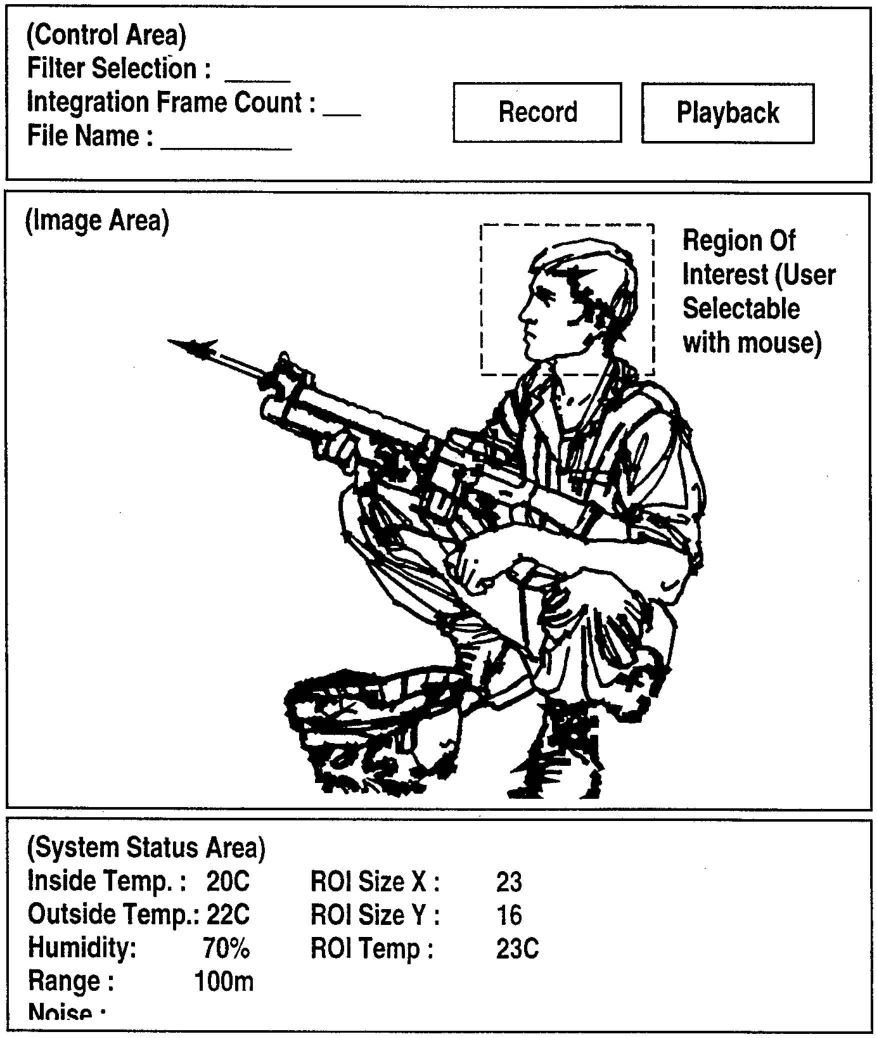

7.5.3 Subsystem Input / Output

The Subsystem Input / Output component will handle all interfacing with the electronic components shown in figure 22. This includes:

- Interfacing with the frame grabber board resident on the PCI bus of the host PC to accept image data from the ISI FPA
- Storage of the image data to the host PC hard drive
- Retrieval of image data previously stored on the host PC hard drive
- Interfacing with the Weather Monitor to accept environmental data (temperature and humidity)
- Interfacing with the Filter Controller to select the proper IR passband filter

7.5.4 Image Processing

The Image Processing component will process the image data. This may include:

- Superpixel calculation
- Atmospheric and background look up table (LUT) processing
- Region of interest sensor response versus temperature calculation

- Image correction
- Calibration processing
- Noise calculation -

7.5.5 Data Storage Capabilities

Each image frame contains 160 x 120 pixels and each pixel contains 14 bits of information (minimum 2 byte of storage required for each pixel). Therefore 38,400 bytes of storage are required for each 160 x 120 image frame. For each gigabyte of hard drive storage, approximately 28,000 image frames can be stored. Most host PC's are configured with at least 4-8 gigabytes of hard drive data storage and the cost for extra storage is relatively inexpensive. Based in this information, it is not anticipated that data storage capacity will become a limitation of the system.

8.0 CONCLUSIONS AND RECOMMENDATIONS

8.1 Phase I Accomplishments

During this Phase I work effort, we verified the feasibility of making a color temperature measurement using two infrared interference filters with neighboring passbands and taking the normalized difference between the two channels. This difference signal measures the shift in the center wavelength of the Planck profile associated with the temperature of the target. We demonstrated this measurement technique with a breadboard scale thermographer system composed of a 10" f/4.5 Newtonian telescope, off the shelf IR filters from OCLI, and an uncooled amorphous silicon microbolometer detector. The chopped signal was recovered with a lock-in amplifier. The Phase I tests measured the system response of a controlled blackbody at a standoff of 102 feet. We also measured NEΔT, accuracy, FOV, and made a human skin temperature measurement at this standoff.

Other work accomplished during the Phase I include designing a calibration routine which, in this case, will correct for attenuation of the target's radiance due to water vapor in the measurement path as well as for errors due to changes in the sensor's internal temperature. The Phase II system will automate these corrections as part of its normal operation mode. We also formulated a system cost model of the proposed Phase II system; we present costs for both the imaging and non-imaging options and also present a forecasted cost which predicts a substantial cost reduction in the FPA and the laptop with PCI slots.

During the Phase I Continuity activities, we carefully reviewed our Phase I test results and made any necessary recommendations for the Phase II work effort. Such recommendations include better characterization of the background radiance as well as further study in the system's measurement repeatability. We made recommendations concerning correcting for atmospheric attenuation, calibration, temperature logging, and system aiming with regards to the Phase II plans. Finally, we present a Phase II Conceptual Design for all of the main sub-systems.

8.2 Areas of Concern

Areas of concern identified during the Phase I work include the issue of background radiation and its effect of the temperature measurement. Depending on the opto-mechanical design, measurement of this quantity may be essential for making an accurate target temperature measurement. However, we believe it is feasible to design the opto-mechanical system such that *only* the incident radiation from the target is modulated by the chopper through careful implementation of baffling and design and placement of the chopper. In this case, only the amplitude modulated signal synchronous with the chopper frequency will be detected and all other background radiation will be rejected. We have identified this as a critical area which will be breadboarded early on in the Phase II.

One potential area of concern to the customer may be the overall size of the proposed Phase II instrument. The anticipated standoff for this application has grown in scope from the original proposal to 1 km. The aperture diameter of the telescope, which dictates the overall size of the instrument, can be reduced in proportion to the maximum standoff range at which the specified system performance must be achieved. For example, if the maximum range were reduced from 1 km to 500 m, then the telescope aperture could be reduced to 8 inches with a corresponding reduction in size of the overall telescope. This de-scope would also be accompanied by a substantial reduction in cost of the telescope.

8.3 Phase II Prospects

At this time, we feel the Phase II prospects are quite good. We have clearly demonstrated that this color temperature measurement is feasible and have presented a Conceptual Design of the Phase II prototype which builds on this concept in an imaging configuration incorporating an uncooled microbolometer focal plane array. During past and present research programs we have accumulated a considerable amount of experience in designing and fabricating telescopes as well as in infrared spectroscopy. We also have immediate experience with the proposed FPA and imaging engine which we used in another recent SBIR Phase II work effort. With our thorough consideration for atmospheric effects as well as background radiation, we believe we have every capability to develop an extremely useful thermographer instrument for the U.S. Air Force.